Pre-sizing of a modular high power density DC/DC converter with GaN components

Lucas Pniak, Bertrand Revol, Loïc Quéval, Jean-Sylvio Ngoua Teu Magambo, Olivier Béthoux

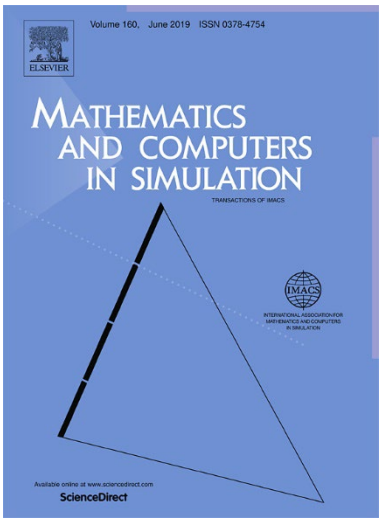

Pre-sizing of a modular high power density DC/DC converter with GaN components

Lucas Pniak, Bertrand Revol, Loïc Quéval, Jean-Sylvio Ngoua Teu Magambo, Olivier Béthoux

DOI: 10.1016/j.matcom.2023.03.028

Reference:

Publisher: ELSEVIER

To appear in: ***Mathematics and Computers in Simulation***

Received date: 14 October 2022

Revised date: 24 February 2023

Accepted date: 22 March 2023

Date of Publication: 2 April 20239 (online)

Volume vvv, month 2023, Pages ppp-ppp

Please cite this article as: Lucas Pniak, Bertrand Revol, Loïc Quéval, Jean-Sylvio Ngoua Teu Magambo, Olivier Béthoux, Pre-sizing of a modular high power density DC/DC converter with GaN components, Mathematics and Computers in Simulation, 2023, , ISSN 0378-4754, https://doi.org/10.1016/j.matcom.2023.03.028.
(https://www.sciencedirect.com/science/article/pii/S0378475423001337).

Document Version: Early version, also known as pre-print

Pre-sizing of a modular high power density DC/DC converter with GaN components

Lucas Pniak[a,b], Bertrand Revol[a], Loïc Quéval[b], Jean-Sylvio Ngoua Teu Magambo[a], Olivier Béthoux[b]

[a] *Safran Tech, Rue des jeunes Bois, Châteaufort, 78117, , France*
[b] *Université Paris-Saclay, CentraleSupélec, CNRS, Laboratoire de Génie Electrique et Electrotechnique de Paris, , Gif-sur-Yvette, 91190, , France*

Abstract

Finding the most appropriate architecture to achieve a function is a major engineering challenge. In the power conversion context, the question that arises is: what is the best trade-off between an architecture based on a single high-power converter and another based on the combination of multiple low-power converters? This article aims to answer this question in the specific case of the isolated interface between the low voltage (28 VDC) and high voltage (±270 VDC) buses of an aircraft. Towards this goal, the targeted power electronics converter is carefully modelled in order to obtain an accurate and fast computing model. A technological database of the different usable components is then used to feed an optimization algorithm. The execution of the latter achieves an attractive and robust result showing an excellent performance in terms of power-to-weight ratio, which is the key index of this study. The precision and speed of this computer-aided design is based on analytical models that are quick to run and therefore enable exploring almost exhaustively the search space. More specifically, the high-frequency transformer has a large relative mass and generates significant losses that are difficult to assess. A major modeling effort has been undertaken and has enable to define a simplified but convincing and accurate model (successfully assessed on a wide bandwidth using an experimental setup). It was used for the first time in this optimization process. According to the targeted aeronautical specifications, the two best solutions would make it possible to achieve a mass power density of 4.5 kW/kg, i.e. twice as high as traditional solutions. This result very clearly shows that the appropriate use of the new GaN transistors makes it possible to make a technological breakthrough. Considering the voltage and current ratings of these components, this shows that the combination of multiple partial converters is very promising and will make it possible in the future to achieve a significant increase in the compactness of electrical power conversion functions. This sizing study therefore clearly shows the potential of the standardized design of power electronics converters and the search for the best combinations (series, parallel) to meet any specific specifications. Additionnaly, the developed approach, based on a modelling effort, especially as far as the high-frequency transformer is concerned, and collection of manufacturer data, also makes it possible to limit the implementations and associated tests.

Hence, the main contributions of this article are i) the assembly of the analytical models of the various components constituting an isolated DC-DC power supply, ii) the simplification of an analytical model of the planar HF transformer, its experimental validation and its first use in a loop of optimization, iii) the fact of showing supporting figures that GaN technology enables technological breakthroughs to achieve high power density, which opens the way to modular architectures based on partial converters of electrical power, iv) the comprehensive description of a powerful pre-study design tool enabling to greatly reduce power converters' time to market.

Keywords: Dual Active Bridge, GaN, Planar transformer, Modelling, Optimization, Aeronautical application.

1. Introduction

For reasons of energy efficiency, reliability and low cost maintenance, the aeronautical industry is gradually moving towards More Electric Aircraft (MEA), i.e. with all on-board equipment powered by electrical energy rather than pneumatic and hydraulic energies [1]. Without having fully switched to electric ancillaries, the Boeing 787 or the Airbus A380 and A350 airliners are 3 current MEA implementations. This new paradigm involves rethinking the electrical power supply architectures of the aircraft in order to ensure the best performance with respect to the key criteria of on-board mass, reliability and resilience [2] [3]. Specifically, the electric power architecture is based on

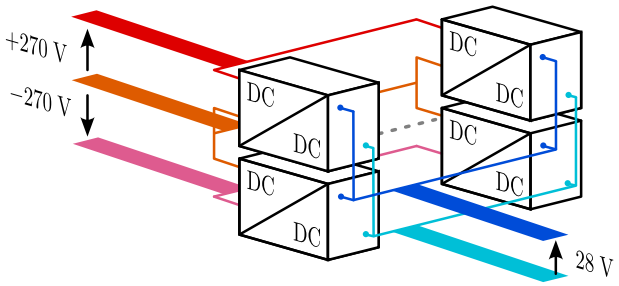

Figure 1: Schematic representation of the modular converter with Input Series Output Parallel associations of the elementary brick to achieve the 540 V — 28 V conversion.

multi on-board grids both interconnected for redundancy purpose and galvanically isolated for safety and reliability reasons [4, 5]. In addition, network voltage levels are quite different: 28 VDC is the standard Low Voltage DC bus (LVDC) dedicated to the control devices while 270 VDC or 540 VDC are devoted to the powerful actuators. It is also important to note that extensive considerations are aimed at further increasing the voltage of the High Voltage DC bus (HVDC): voltages of 800 V or even more are envisaged. In this context, aeronautical manufacturers have to carefully design power electronics converters [6], which are the key components permitting to interface LVDC and HVDC networks and accurately control the power flowing between them. This work aims to establish an effective method to accelerate the design stage.

Simultaneously with this evolution on the more electric aircraft, power electronics components diversity is significantly and rapidly evolving with the arrival at maturity of Wide Band Gap (WBG) technologies [7] such as Silicon Carbide (SiC) [8] and Gallium Nitride (GaN) [9, 10]. Compared to standard silicon (Si) devices, these novel components stand higher junction temperatures enabling to decrease the heat sink size. They also faces lower losses both regarding conduction and switching ones. Such lower power losses both contributes to enhance the conversion efficiency and reduce the thermal management system size. However, the voltage and current ratings of these components do not enable them to be directly substituted for conventional ones. To achieve the expected function, it is therefore necessary to consider modular architectures based on the series and/or parallel connection of lower power elementary bricks [11, 12, 13], see Figure 1. This work addresses the issue of well quantifying the benefits of switching from a single converter based on directly adapted components to a multi-converter structure adopting the most appropriate components to achieve a given specification.

To address this issue, a numerical tool is developed. As technology evolves rapidly, it is vital to be able to repeat this procedure frequently in order to consider technological developments without carrying out long and costly implementations and tests. Reducing developments cost as well as time to market has indeed become a key issue. The two arising challenges are therefore to produce a simulation design tool giving relevant orders of magnitude, in order to make a relevant implementation decision, and making it possible to process a large number of parameters and possibilities in a short time.

To test the developed Simulation-Based Design tool dedicated to power electronics converters, the interconnection between LVDC and HVDC networks was chosen. This is a particularly critical case because i) the related voltage level ratio is large (around 20), ii) the link has to be power reversible and iii) voltage isolation is mandatory. The studies presented in the literature show that it is possible to reach power to weight ratios of 1 to 1.5 kW/kg by exploiting SiC semiconductors on the high voltage side and Si on the low voltage side [14], about 2 kW/kg with a mixed SiC/GaN design [15]. With a modular architecture (Figure 1), the use of only GaN semiconductors becomes possible, so that the power density can be further increased. Among the possible topologies for the elementary brick [16], the Dual Active Bridge (DAB) converter, shown in Figure 2, meet the requirements of galvanic isolation, high power density, high power ratings and high efficiency [4, 17]. Several studies also show that it is suitable for series and parallel connection thanks to its current source behavior [18, 19]. The Dual Active Bridge was therefore selected for the elementary brick of the modular converter and comprehensively studied for the proof of concept. More precisely, its specifications are given in table 1.

When it comes to the MEA, aerospace manufacturers are facing challenges in developing smaller and lighter

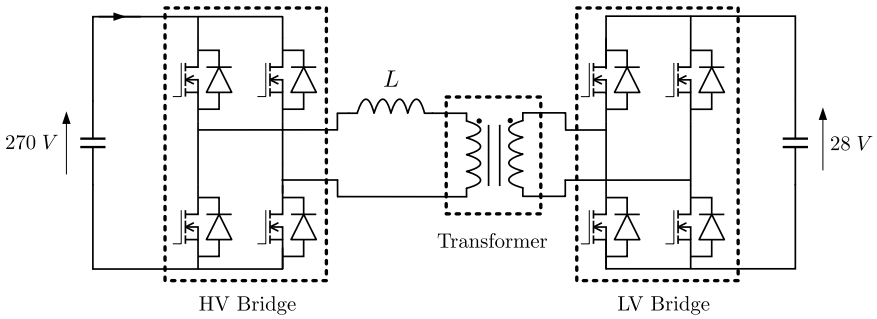

Figure 2: Schematic of the Dual Active Bridge converter.

Table 1: Dual Active Bridge converter specifications

Parameter	**Nominal value**	**Range of variation**
Input voltage V_e	270 V	[210; 330] V
Output voltage V_s	28 V	[16; 32] V
Rated power P	to be determined between 1 and 5 kW	

electric power systems, to truly achieve the weight reduction benefit induced by replacing hydraulics and pneumatics with electrics. Consequently, this article adopts the power density as the only performance index. To clarify the basis of the optimization carried out, all the analytical models permitting to estimate losses and masses are detailed. Similarly the models related to the constraints governing the power converters are specified. Additionally, it is shown that greatest modeling efforts focus on the transformer. Indeed, the high primary - secondary voltage ratio enforces the windings parallelization on the low voltage side, which greatly complicates the copper losses assessment. In this regard, an energy approach enables to provide a precise model which remains simple to implement and configure. The optimization is conducted with a Particle Swarm Optimization (PSO) algorithm [20, 21, 22]. The results presented in this article show that the GaN-based elementary brick can reach a 4.5 kW/kg power density, which is more than twice as high as what can be achieved with converters based on SiC or Si technologies ($\sim$ 2 kW/kg).

This article is organized as follows. Section 2 introduces the global scheme of the optimization process. It specifies the cost function to be optimized and the various tuning parameters. Then, section 3 describes comprehensively the power loss and mass estimation models. Section 4 presents the design constraints of the elementary brick and its components. The related models are detailed. Section 5 outlines the findings of the optimization run and shows a partial experimental validation. Section 6 draws the main conclusions and perspectives of the current work.

2. Simulation-Based Design

This study aims to provide a methodology for power electronics converters designers to define, by computation and before any implementation, the key parameters that their power architecture should have based solely on its specifications. The three main elements to be considered in this decisive design stage are described in this section and explained in the considered case study, namely the optimization of a high voltage ratio DAB converter. To this end, the desired purpose is first described (subsection 2.1.) to finally explain the action levers to achieve it (subsection 2.3.). Obviously, to undertake the optimization process, it is mandatory to explain the formal links that link the means to the desired end as well as the databases necessary for using these formal relationships (subsection 2.2.). Figure 3 illustrates the procedure of the method thus described.

2.1. Objective function

As aforementioned one of the remaining challenges of MEA is to achieve weight saving. This goal is a key point since mass is the main airplane fuel consumption driver while the payload is what an airline can sell. With this respect,

the current study is based on the power-to-weight ratio P_m as a single cost function. It is written as follows :

$$P_m = \frac{P - \Sigma P_i}{\Sigma M_i} \tag{1}$$

where P is the converter rated power, P_i are losses in its various components, and M_i are the mass of each constituent.

Note that the electrical conversion efficiency is necessarily taken into account by this performance index because mass and volume of a converter are strongly determined by its losses. As a sum, the design algorithm requires on accurate models computing the losses and the masses of each elementary part.

2.2. Algorithm architecture

Solving an optimization problem requires significant computational resources, especially since the models used are numerically complex to solve and the search space is large (high number of optimization parameters and substantial variation ranges). This is indeed the case of this study. On one hand it aims providing an effective and therefore precise means of avoiding long and costly trial and error process. Secondly, it seeks to explore all the possibilities for converging towards ultra-relevant technology elementary bricks enabling the products standardization by modules combination. To achieve fast computing, the models used by the PSO optimization algorithm are analytical ones. Additionally, the considered design parameters can be either discrete or continuous variables.

2.3. The selected case study

As mentioned in the introduction section, the selected case study focuses on the most relevant DAB converter permitting to achieve a macro-converter interfacing the aircraft LVDC and HVDC buses. Its rated power and switching frequency are typical macro-parameters that have to be set by the optimization process. More specifically, eleven design parameters are considered. They could be classified in 3 categories: global operating parameters, active bridge settings and transformer characteristics. All the information are summed up in Table 2. Additionally, Figure 3 shows the general schematic of the simulation-based design tool, developed and evaluated on a DAB used for power management purposes in an embedded microgrid.

Table 2: Design parameters

Category	**Symbol**	**Parameter**
DAB operating parameters	f	Switching frequency
	L	DAB inductance value
Geometric parameters of the transformer	FCR	Ferrite Core Reference
	e_c	Conductor thickness
	d_{pp}	insulator thickness between conductor of the same winding
	d_{ps}	insulator thickness between conductor of different winding
	e_0	air gap thickness
	WIC	Winding Interleaving Configuration
Parameters related to the bridges	HVGaN	HV bridge GaN reference
	LVGaN	LV bridge GaN reference
	N_1	Number of transistors in parallel in the HV bridge
	N_2	Number of transistors in parallel in the LV bridge

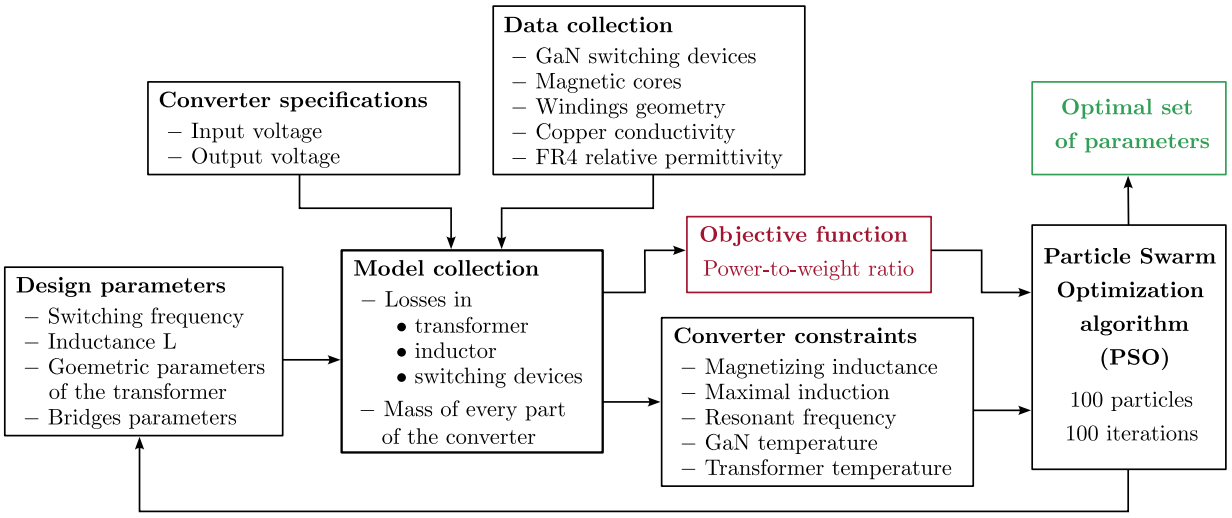

Figure 3: Schematic illustration of the developed method to find the most compact elementary brick enabling to achieve the desired modular macro converter.

3. Converter modeling

The purpose of this section is to describe the collection of models needed to estimate the power to weight ratio of the Dual Active for a given set of parameters. According to the equation (1), this requires an estimate of the rated power of the DAB, the various losses it experiences and the mass of each of these components. They are detailed in the following subsections.

3.1. DAB rated power

The electrical power conversion function is performed by a combination of elementary bricks. These are based on DAB technology and controlled using a single-phase-shift (SPS) control strategy. The latter is the standard control technique consisting in driving both the LV and HV bridges by a square wave (with 50% duty-cycle) and adjusting its power p by tuning the normalized phase-shift ϕ in the range $[-0.25, 0.25]$. Using SPS and assuming zero losses, the power transfer from one DC bus to the other one p is determined by the following equation [23]:

$$p(\phi) = \frac{mV_pV_s}{fL}\phi(1 - 2|\phi|) \tag{2}$$

where m is the transformer ratio, f is the switching frequency, V_p and V_s are the nominal voltage of the DC networks and L is the inductance in series with the transformer. The rated power of the Dual Active Bridge converter P is reached when $p(\phi)$ is maximal, corresponding to $\phi = 0.25$. It gives:

$$P = \frac{mV_pV_s}{8fL}. \tag{3}$$

The inductor L mass and volume strongly depend both on LP^2 and also on the quantity of magnetic heat losses to be removed. The core material used as well as the switching frequency f selected highly impact these losses. Likewise, the switching frequency f deeply affects the auxiliary power derived to operate the GaN drivers. By this single equation (2), it could therefore already been perceived that the addressed problem of minimizing the power-to-weight index is highly entangled. Subsequently, DAB modeling requires particular care. The present section and the following one deal with this demanding issue.

3.2. Loss models

3.2.1. In semiconductors

Conduction losses. High Voltage (HV) and Low Voltage (LV) bridges suffer various losses. Among them, the most significant are the transistors conduction losses $P_{c,i}$. They are modeled based on the on-state resistance $R_{DS_{on}}$ of the GaN components, the number of components in parallel and the shape of the current $i_L(t)$ passing through the inductor L , as described in [24, 17]. The $R_{DS_{on}}$ value specified at the quite high temperature of 125°C is considered in order to provide a representative insight in the toughest conditions.

$$P_{c,1} = \left(\frac{4}{N_1}\right)\frac{R_{DS_{on},1} I_L^2}{2}, \tag{4}$$

and

$$P_{c,2} = \left(\frac{4}{N_2}\right)\frac{R_{DS_{on},2}(NI_L)^2}{2}, \tag{5}$$

where N is the transformer ratio, N_1 and N_2 the number of of GaN components in parallel per switch and I_L the rms current in the inductor L.

Switching losses. The DAB converter naturally achieves Zero Voltage Switching (ZVS). It makes the switching losses $P_{sw,i}$ negligible, at least with regard to the HV bridge. The LV bridge is a more complicated issue. In case the parasitic inductance of the LV bridge power loop is too large, the high level of switched current (between 100 and 200 A) may induce significant losses [17]. These losses are strongly dependent on the routing technology and are therefore difficult to estimate. In the first instance, these aspects had been overlooked and the related losses neglected. It could be refined in the final design stage.

$$P_{sw,1} = P_{sw,2} = 0. \tag{6}$$

Reverse conduction losses during dead times. During the dead time phases $t_{dt,i}$, the GaN component naturally conducts the switched current $I_{sw,i}$ in reverse. This switched current is supposed constant as the dead time is very short compared to the switching period $1/f$. It can be calculated using the expressions provided in [25]. The drain-to-source voltage $V_{ds,off,i}$ drop can then be estimated using the reverse conduction characteristics of the GaN component extracted from the datasheet. It depends on the gate-to-source blocking voltage and on the switched current value. This phenomenon of reverse conduction induces important losses $P_{dt,i}$ which are expressed as follows. Regarding the dead time short duration, the related energy losses may be fairly low.

$$P_{dt,i} = 4V_{ds,off,i} I_{sw,i} t_{dt,i} f, \quad i = 1, 2. \tag{7}$$

Gate charge losses. At each switching period, the driver applies a voltage variation $\Delta V_{gs,i}$ to the gate of the transistors to turn them on. It supplies a charge Q_g according to the gate charge characteristic given in the datasheet. In accordance with [26], the power dissipated in this process is given by equation (8).

$$P_{g,i} = 2\Delta V_{gs,i} N_i Q_{g,i} f, \quad i = 1, 2. \tag{8}$$

3.2.2. In magnetic components

The transformer implementation considered in this study is planar technology. Thanks to their numerous advantages [27, 28], planar transformers meet the demanding requirements of modern power electronics, especially in terms of high operating frequencies and power density [29]. Indeed, the flat shape of its windings enables a quite homogeneous current distribution within the entire turns cross-section. More specifically this property is attractive at high frequency avoiding the impact of skin effect and proximity effects [30]. Like any magnetic component, it is however impacted by two types of losses: iron losses and copper losses.

Iron losses. Iron losses are classically described using the Steinmetz formula [31, 32],

$$P_{tr,fer} \simeq V_{tr,fer} k f^{\alpha} \hat{B}_{amp}^{\beta} \tag{9}$$

with k, α and β being the Steinmetz parameters obtained from the values given in the datasheet of the magnetic materials used (least squares approximation), $V_{tr,fer}$ the volume of magnetic material and $\hat{B}_{amp}$ the maximum amplitude of the magnetic induction. $\hat{B}_{amp}$ is estimated using the Maxwell-Faraday Law. Considering that the LV winding composed of n_2 turns is subjected to a square wave voltage of amplitude V_2, the induction $\hat{B}_{amp}$ in the transformer of core section S_f is expressed as follows:

$$\hat{B}_{amp} = \frac{V_2}{4 n_2 f S_f} \tag{10}$$

Copper losses. When no windings parallelization is considered, Dowell's and Ferreira's models [33, 34] provide good estimates of copper losses $P_{tr,copper}$. However, regarding the considered use case, the high transformer ratio causes the LV side undue hardship. To overcome the LV excessive current density and limit copper losses, parallel windings are obviously mandatory. At high frequency, the correct distribution of the currents in these windings is no longer certain and must be thoroughly assessed. To this purpose, a simplified version of the harmonic model presented in [35] is developped in this paper. The approach is quite similar to the method proposed by Weichen in [36], but much easier to implement. It is based on a well-known physical principle called "principle of least action". Applied to electrokinetics, it states that "electric current flows along the path of least impedance" [37]. For the purpose of addressing the transformer copper issue, a short-circuit is set, for instance on the LV side of the transformer. In this case, a sinusoidal current of magnitude I_0 and pulsation ω is enforced in the primary winding, i.e. on the HV side, as represented in Figure 4. The transformer acts then as an impedance $\underline{Z}_t$ composed of the windings AC resistance R_{ac} and the windings leakage inductance L_{ac}. It can be written as:

$$\underline{Z}_t = R_{ac} + j L_{ac} \omega. \tag{11}$$

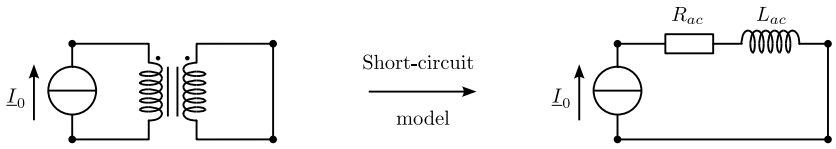

Figure 4: Equivalent circuit model of a short-circuited transformer excited by an harmonic current source $\underline{I}_0$.

Copper losses in transformer windings are estimated based on R_{ac} which has to be accurately determined. The latter, as well as L_{ac}, highly depends on the current distribution in the windings connected in parallel as it is demonstrated in [35]. Noting $\underline{I} = [\underline{i}_1 \dots \underline{i}_N]^T_{N\times 1}$, the vector of the complex currents in each of the N copper layers of the transformer defined in Figure 5, R_{ac} and L_{ac} are the following:

$$R_{ac} = \frac{\underline{I}^{\dagger} R \underline{I}}{|\underline{I}_0|^2}, \tag{12}$$

and,

$$L_{ac} = \frac{\underline{I}^{\dagger} L_{lk} \underline{I}}{|\underline{I}_0|^2}, \tag{13}$$

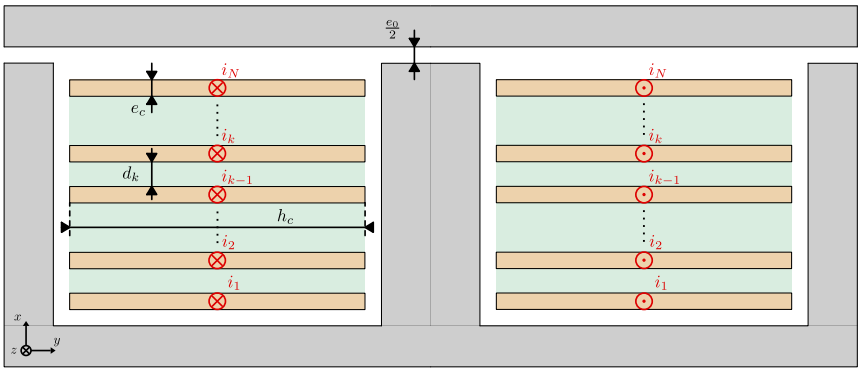

Figure 5: Cross-sectional representation of a planar transformer with N conductor layers. The magnetic circuit is represented in gray, the conductors in copper color and the insulators in green.

where † is the transpose conjugate operator. According to [35], the resistance matrix R is expressed as follows

$$R = \frac{L_c}{\sigma \delta h_c} T^{\dagger} \underbrace{\begin{pmatrix} A_J & -\frac{B_J}{2} & & & (0) \\ -\frac{B_J}{2} & 2A_J & -\frac{B_J}{2} & & \\ & \ddots & \ddots & \ddots & \\ & & -\frac{B_J}{2} & 2A_J & -\frac{B_J}{2} \\ (0) & & & -\frac{B_J}{2} & A_J \end{pmatrix}}_{\text{Size } (N+1)\times(N+1)} T, \tag{14}$$

with

$$A_J(\Delta) = \frac{\sinh(2\Delta) + \sin(2\Delta)}{\cosh(2\Delta) - \cos(2\Delta)}, \tag{15}$$

$$B_J(\Delta) = 4\frac{\cos(\Delta)\sinh(\Delta) + \cosh(\Delta)\sin(\Delta)}{\cosh(2\Delta) - \cos(2\Delta)} \tag{16}$$

$$\Delta = e_c/\delta. \tag{17}$$

and L_c the mean length of one winding turns, h_c the conductor layers width, σ the conductor conductivity, δ the skin depth at the pulsation ω in a material of permittivity μ_0,

$$\delta = \sqrt{\frac{2}{\mu_0 \sigma \omega}}, \tag{18}$$

and T a matrix defined as follows:

$$\mathrm{T} = \begin{pmatrix} 0 & \dots & 0 \\ 1 & & (0) \\ \vdots & \ddots & \\ 1 & \dots & 1 \end{pmatrix}_{(N+1)\times(N)}. \tag{19}$$

Referring to [35], the leakage inductance matrix L_{lk} is expressed as follows

$$L_{lk} = T^{\dagger} \left(\frac{L_c h_c}{\sigma \delta \omega} \begin{pmatrix} A_{lk} & -\frac{B_{lk}}{2} & & & (0) \\ -\frac{B_{lk}}{2} & 2A_{lk} & -\frac{B_{lk}}{2} & & \\ & \ddots & \ddots & \ddots & \\ & & -\frac{B_{lk}}{2} & 2A_{lk} & -\frac{B_{lk}}{2} \\ (0) & & & -\frac{B_{lk}}{2} & A_{lk} \end{pmatrix} + \mu_0 L_c h_c \begin{pmatrix} d_1 & & & (0) \\ & d_2 & & \\ & & \ddots & \\ (0) & & & d_{N+1} \end{pmatrix} \right) T, \tag{20}$$

where d_k are insulator layers thickness defined in Figure 5, and

$$A_{lk}(\Delta) = \frac{\sinh(2\Delta) - \sin(2\Delta)}{\cosh(2\Delta) - \cos(2\Delta)} \tag{21}$$

$$B_{lk}(\Delta) = 4\frac{\cos(\Delta)\sinh(\Delta) - \cosh(\Delta)\sin(\Delta)}{\cosh(2\Delta) - \cos(2\Delta)}. \tag{22}$$

The impedance of the transformer in short circuit can then be expressed as a function of the current vector in each of the layers:

$$\underline{Z_t} = \frac{\underline{I}^{\dagger}(R + jL_{lk}\omega)\underline{I}}{|\underline{I_0}|^2}. \tag{23}$$

Note that I_0 is the magnitude of the sinusoïdal current enforced in the HV winding as described in the first paragraph of this section. According to the principle of least action, the currents flow through the path of least impedance. Consequently, the currents flowing in the parallel connected windings distribute in a way that minimizes $\underline{Z_t}$. On the contrary, the currents flowing in the turns of the high voltage winding are imposed by the source $\underline{I_0}$, and are constraints of the impedance minimization problem:

$$\forall k \in \text{the HV winding}, \quad \underline{i_k} = \underline{I_0}. \tag{24}$$

Also, assuming a perfect coupling between the two windings (no magnetizing current), the current I_0 coming into the primary winding is equal to the current going out of the secondary winding. According to the definition of the currents i_k in each turn of the windings (Figure 5), this results in the sum of the N currents being zero:

$$\sum_{k=1}^{N} \underline{i_k} = 0. \tag{25}$$

These M constraint linear equations on the currents (Equation (24) and (25)) can be written in matrix form defining a matrix A (size $M \times N$) and a source current vector $\underline{I_s}$ (size $M \times 1$ containing $\underline{I_0}$) :

$$A\underline{I} = \underline{I_s}. \tag{26}$$

The explicit expressions of the matrices A and Is then depend on the distribution of the primary and secondary turns on the different layers of the planar transformer.

The problem of minimizing the impedance $\underline{Z_t}$ under linear constraints can then be solved using Lagrange multipliers approach. The method principle is as follows: in order to find the minimum of the function $\underline{Z_t}(\underline{I})$ subjected to the constraint $A\underline{I} - \underline{I_s} = 0$, the Lagrangien function $\mathcal{L}(\underline{I}, \underline{\lambda})$ is defined as :

$$\mathcal{L}(\underline{I}, \underline{\lambda}) = \underline{Z_t}(\underline{I}) + \left(A\underline{I} - \underline{I_s}\right)^T \underline{\lambda}. \tag{27}$$

The solution of the impedance minimizing problem is the stationary point of $\mathcal{L}$ as a function of $\underline{I}$ and $\underline{\lambda}$. This means that the partial derivatives of $\mathcal{L}$ with respect to these variables must be zero, including the partial derivative with respect to $\underline{\lambda}$. The calculation of these partial derivatives enable to express the system to be solved to determine the currents:

$$\begin{cases} \left[R + j\omega L_{lk}\right]\underline{I} + A^T\underline{\lambda} = 0 \\ \\ A\underline{I} = \underline{I_s} \end{cases} \tag{28}$$

Thus, for each set of parameters, the linear system (28) is solved to obtain the value of the currents $\underline{I}$, which is injected into (12) to estimate the ac resistance and thus the AC copper losses.

3.3. Mass estimation models

Full bridges PCBs and the related heatsink. In such pre-sizing phase, it is rather difficult to determine a full-bridge mass. Many elements are not yet well established, such as driver components, connectors, PCB surface, track size. In

this context, the partial mass of these components is computed based on previous H-bridge designs. The PCB mass is assessed as a function of the number of GaN components in parallel per switch. To ensure proper heat dissipation and hence thermal management, a single heat sink is set on each of the two H-bridges. Depending on the power dissipated by the bridge and the number of transistors in parallel per switch, the minimum thermal resistance $R_{th_{min}}$ between the heat-sink and the air is computed. A thorough analysis of various datasheets provided by aluminium heat-sink manufacturers permits to determine a rather invariant quantity σ_m. The latter is the thermal conductance mass density. In the case of a 4m/s forced ventilation, it equals:

$$\sigma_m = 50 \text{ W/(Kkg)} \tag{29}$$

Subsequently, we propose the following estimation of heat-sinks masses:

$$M_{heatsink,i} = \frac{1}{\sigma_m R_{th_{min},i}}, \quad i = 1, 2. \tag{30}$$

Inductor. The DAB series inductor mass is also assessed based on data provided in manufacturers datasheets. A large number of high current rating inductors enables to establish another roughly invariant quantity: Φ_m, the maximum flux per unit of mass. We express it as follows:

$$\Phi_m = \frac{LI_{sat,10\%}}{M_{ind}} \simeq 6,7 \text{ Wb/kg} \tag{31}$$

where $I_{sat,10\%}$ is the saturation current corresponding to a 10% drop in the rated inductance L. Thus, an inductor, characterized by an inductance value L and a rated maximum rms current $I_{L,max}$, has an estimated mass M_{ind} defined by:

$$M_{ind} = \frac{L\beta I_{L,max}}{\Phi_m} \tag{32}$$

where β is a safety factor greater than 1.0 depending on the current waveform. A $\beta = 1.5$ is considered since the maximum current carried by the inductor never exceeds 30% of its rms value I_L at maximum power.

Planar transformer. The planar transformer mass M_{tr} is related to the volume V_i and mass densities ρ_i of the various materials constituting the transformer. Among the components are the magnetic material, the copper and the PCB dielectric material, namely FR4. M_{tr} is then expressed as follows :

$$M_{tr} = \sum_{\text{ferrite,copper,FR4}} \rho_i V_i. \tag{33}$$

Note that the volumes V_i are calculated using the geometrical parameters of the transformer.

4. Physical and geometric constraints

To complete these physical models and to finish the modeling of this Dual Active Bridge, it is necessary to consider the physical constraints that apply to its parameters. These constraints will define the boundaries of the optimization problem solved in this paper. Most of them concern the transformer (magnetic saturation of the core, minimal magnetizing inductance value, minimal resonant frequency or maximum winding thickness), but the thermal constraints on GaN components are also described. They are all detailed in this section.

4.1. Transformer constraints

Magnetic saturation. The induction magnitude B_{amp} in the central core leg (having a S_f section surface) must not exceed the maximum induction chosen by the program user. This maximum induction is chosen regarding the magnetic material characteristics. The constraint basic purpose is preventing any saturation in the magnetic material. In order to take into consideration the high frequency core losses, $B_{max} = 0.2$ T is considered for a 3C95 material. The latter is selected for its attractive performance at the desired frequency range. Considering that a square wave of amplitude V_2 applies on the LV winding composed of n_2 turns, the inequality constraint is [17]:

$$B_{amp} = \frac{V_2}{4n_2 f S_f} \leq B_{max} \tag{34}$$

Magnetizing inductance value. The HV magnetizing inductance L_{m_p} [30] has to be larger than the DAB series inductance L by a factor k_L. The latter is specified by the program user. This factor must be sufficiently large so that the reactive power exchanged with the transformer remains negligible compared to the active power exchanged through the series inductance. A choice of $k_L = 8$ strongly limits this reactive power while enabling low magnetizing inductance values, which is necessary to fulfill the resonant frequency constraint. Thus,

$$L_{m_p} = \frac{A_L n_1^2}{1 + \mu_r \frac{e_0}{L_\gamma}} \geq k_L L, \tag{35}$$

where A_L is the core specific inductance (without any air gap), n_1 is the number of turns of the HV winding, e_0 is the thickness of the air gap, μ_r is the core material relative permeability, and L_γ is the average length of the magnetic circuit.

Resonant frequency. To guarantee the correct operation of the transformer, its open circuit resonance frequency f_r must be higher than the switching frequency f of the converter. We then impose the following constraint:

$$f_r \geq k_f f, \tag{36}$$

where k_f is a margin coefficient that we set equal to 3.5. To estimate the transformer resonant frequency f_r, a simple equivalent model is established. As shown in Figure 6, the electrical energy stored in the windings is modeled by a simple capacitance C_p brought back to the HV side. The latter mainly interacts with the magnetizing inductance L_{m_p} (large in relation to the leakage inductance L_f) around the resonant frequency which is expressed as:

$$f_r = \frac{1}{2\pi \sqrt{L_{m_p} C_p}}. \tag{37}$$

The parasitic capacitance C_p is computed from the electrical energy stored between each layer of conductors in the winding window. Three distinct cases can be distinguished, namely: two HV winding layers in interaction, two LV winding layers in interaction, and finally interaction between a HV winding layer and a LV winding layer. In the considered winding geometries, the HV winding is composed of n_1 turns while each of its conductor layers is composed of n turns On the contrary, the LV layers build a single turn; they are all connected in parallel. Noting V_1 the voltage applied to the transformer HV winding, d the thickness of the insulator of permittivity $\epsilon_0\epsilon_r$ between two layers of conductor of surface S, the elementary geometrical capacitance C_0 of two turns facing each other may be expressed as:

$$C_0 = \frac{\epsilon_0 \epsilon_r S}{nd} \tag{38}$$

The electrical energy stored between the conductor layers also depends on how the layers are connected to each other, as shown in Figure 7. Therefore, the energy calculation must be done for the continuous winding technique (Figure 7.a) and for the discontinuous winding technique (Figure 7.b) , as in [27].

— *Two HV winding layers - continuous winding.* (Figure 7.a)

$$E_{pp,a} = \frac{1}{2} C_0 \sum_{k=1}^{n} \left((2k-1) \frac{V_1}{n_1} \right)^2 = \frac{1}{2} C_0 \left(\frac{V_1}{n_1} \right)^2 \times n \left(\frac{4n^2 - 1}{3} \right) \tag{39}$$

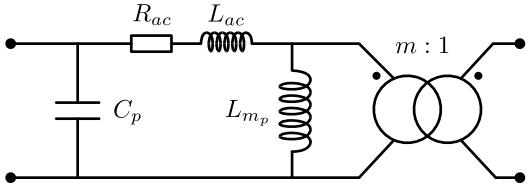

Figure 6: HF equivalent model of the planar transformer. R_{ac} is the equivalent AC resistance of the HV and LV windings brought back to the HV side, L_{ac} the leakage inductance brought back to the HV side, L_m the magnetizing inductance of the HV winding and C_p the parasitic capacitance brought back to the HV side representing the electrical energy stored in the transformer.

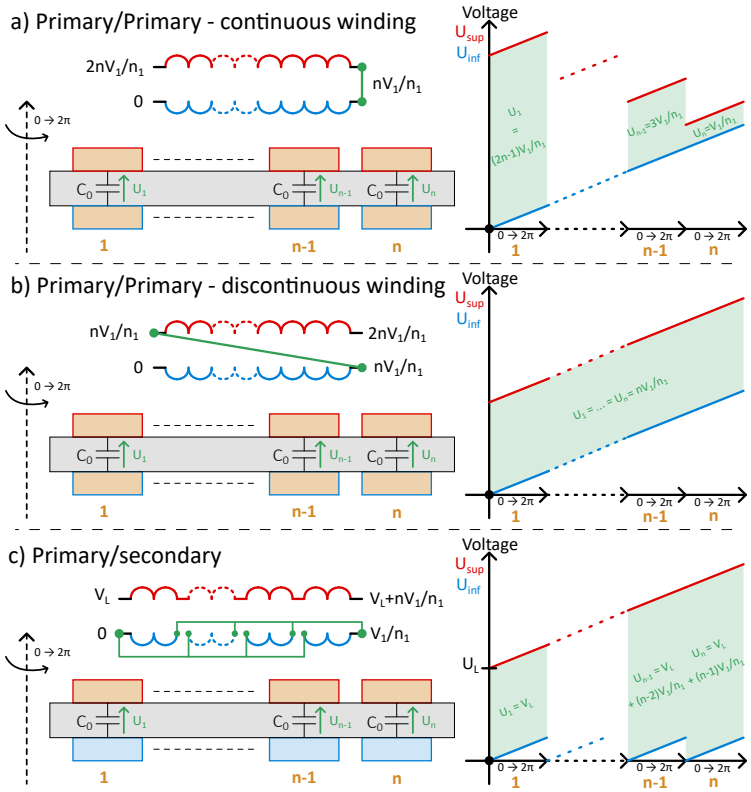

Figure 7: Left side : Possible scenarios of electrical coupling between two layers of conductors. Right side : related potential differences between the facing turns.

— *Two HV winding layers - discontinuous winding.* (Figure 7.b)

$$E_{pp,b} = \frac{1}{2}C_0 \sum_{k=1}^{n} \left(n\frac{V_1}{n_1}\right)^2 = \frac{1}{2}C_0 \left(\frac{V_1}{n_1}\right)^2 \times n^3 \tag{40}$$

— *Two LV winding layers.* As all the LV winding layers are electrically connected in parallel, the potential difference between turns facing each other is zero [27]. It means that there is no electric field in the insulation layer and that the electrical energy stored between two LV winding layers is zero.

$$E_{ss} = 0 \tag{41}$$

— *HV and LV winding layer.* (Figure 7.c) Assuming that, for the i^{th} HV winding layer, the left end is at potential $V_L = (i-1)V_1/n_1$, we have,

$$E_{ps} = \frac{1}{2}C_0 \sum_{k=1}^{n} \left(V_L + [k-1]\frac{V_1}{n_1}\right)^2 = \frac{n}{2}C_0 \left[V_L^2 + (n-1)V_L\frac{V_1}{n_1} + \frac{(n-1)(2n-1)}{6}\left(\frac{V_1}{n_1}\right)^2\right] \tag{42}$$

— *Expression of the equivalent parasitic capacitance referred to the HV side.*

$$C_p = 2\frac{\sum E_{pp} + \sum E_{ps}}{V_1^2} \tag{43}$$

PCB thickness. The PCB thickness e_{PCB} should not exceed the winding window height e_p. Hence, e_{PCB} has to respect the following inequality constraint:

$$e_{PCB} = \sum_{k=1}^{N+1} d_k + N \cdot e_c \leq e_p \tag{44}$$

where N is the number of conductor layers of thickness e_c, and d_k, $k \in [1, N+1]$, corresponds to each insulation thickness between two consecutive conductors.

Thermal dissipation. The power dissipated by the transformer must be lower than the maximum power it can naturally dissipate when it reaches the critical temperature $\theta_{c_{tr}}$ defined by the user. For an ambient temperature of $\theta_{amb} = 20°C$, a heating of 80°C is allowed, that is $\theta_{c_{tr}} = 100°C$. The power dissipated by convection is assessed based on Newton's formula:

$$\Phi_c = h_{conv} S (\theta - \theta_{amb}). \tag{45}$$

where h_{conv} is the convective exchange coefficient depending both on the temperature and exchange surface orientation [38]. Finally, the heating powers that can be handled by convection is computed both regarding ferrite and transformer PCB, namely $\Phi_{c,fer}$ and $\Phi_{c,PCB}$ respectively. Note that at the dimensions and temperatures involved, the heat infrared radiation is negligible compared with the heat transport by convection. Thus, the following constraint must be verified,

$$P_{tr,copper} + P_{tr,fer} \leq \Phi_{c,fer} + \Phi_{c,PCB}. \tag{46}$$

4.2. H-bridges thermal constraints

According to datasheets, the GaN transistors temperature should not exceed the critical value of 150°C. To achieve a reliable safety level, appropriate safety margins have been adopted, choosing $\theta_{j_{max}} = 120°C$ as the maximum temperature threshold.

4.3. Summary

At this stage of the proceeding, all the equations describing the power electronics converter have been established based on analytical formulations. In particular, it is possible to calculate the power to weight ratio, which is the chosen objective function. As aforementioned, its expression can be written as:

$$F_{obj} = P_m = \frac{P - P_{tr} - P_{br,1} - P_{br,2} - P_{ind} - P_{capa}}{M_{tr} + M_{br,1} + M_{br,2} + M_{ind} + M_{capa}} \tag{47}$$

where P is the converter rated power, P_{tr} is the transformer power losses, $P_{br,1}$ is the HV bridge power losses, $P_{br,2}$ is the LV bridge power losses, P_{ind} is the inductor power losses, P_{capa} is the decoupling capacitors power losses, M_{tr} is the transformer mass, $M_{br,1}$ is the HV bridge mass, $M_{br,2}$ is the LV bridge mass, M_{ind} is the inductor mass and M_{capa} is the decoupling capacitors mass. The following section therefore describes the implementation and use of the optimization algorithm based on the models described. This part ends with the analysis of the obtained results in the specific case of a DAB converter.

5. Optimization implementation: results and discussion

5.1. Use Case

An algorithm exploiting these loss and mass estimation models has been developed in order to identify the most suitable converter structure for an elementary brick of a HVDC-LVDC macro-converter. As mentioned, the use case is a high ratio DAB converter. The design parameters are listed in Table 2. One of the answers that the decision-making process must provide is to determine the most suitable power for one DAB. In this study, the optimization algorithm speed benefits from the fact that some variables have limited range. For instance, galvanic isolation is achieved using a planar transformer which is a specific technology, both in terms of dedicated cores and PCB copper thickness [28]. Additionally, GaN transistors are still, for the moment, under development. Consequently the number of references are quite limited. Finally, the series inductor is not custom made but selected from a manufacturer catalogue. Therefore, the overall search space is wide but could be even wider in the future with technology maturity.

5.2. Optimization problem

We look for the DAB converter sizing that minimizes the power to weight ratio P_m. The optimization problem is formulated as follows:

$$\begin{aligned} \underset{X}{\text{minimize}} \quad & P_m(X) \\ X = & \{f, L, \text{FCR}, e_c, d_{pp}, d_{ps}, e_0, \text{WIC}, \text{HVGaN}, \text{LVGaN}, N_1, N_2\} \\ \text{subject to} \quad & B_{amp} \leq 0.2 \text{ T} \\ & L_{m_p} \geq 8L \\ & f_r \geq 3.5f \\ & e_{PCB} \leq e_p \\ & P_{tr} \leq \Phi_c \\ & \theta_{j_{max}} \leq 120°\text{C} \end{aligned} \tag{48}$$

where the optimization variables X are (Table 2): the switching frequency f, the serial inductance of the DAB L, the Ferrite Core Reference FCR, the transformer winding turns thickness (i.e. thickness of the PCB conductor layer) e_c, the insulation layer thicknesses in the transformer winding d_{pp} and d_{ps}, the air gap of the transformer core e_0, the Winding Interleaving Configuration WIC, the HV bridge GaN reference HVGaN, the LV bridge GaN reference LVGaN, the number of transistors in parallel per switch in the HV bridge N_1 and the number of transistors in parallel per switch in the LV bridge N_2. Note that this optimization is conducted with a specific set of constraints. The magnetic induction in the core must remain below 0.2 T. The magnetizing inductance L_{m_p} must be at least 8 times larger than the series inductance L of the DAB. The open circuit resonance frequency of the transformer f_r must be at least 3.5 times greater than the DAB switching frequency f. The thickness of the transformer windings manufactured in PCB technology e_{PCB} must be smaller than the winding window height e_p. The losses in the transformer P_{tr} must be lower than the power that can be dissipated by natural convection Φ_c. And finally, the junction temperature of GaN θ_j components should not exceed 120°C.

The optimization is performed by a Particle Swarm Optimization (MOPSO) algorithm [20, 21, 22] with 100 particles and 100 iterations. With a desktop computer with Intel core i7 10^{th} generation, 1.8 GHz and 16 GB of RAM, one single optimization takes around 10 minutes.

5.3. Results

The main results of executing the described optimization algorithm are shown in Table 3. Each of the A, B and C columns refers to the optimum sizing obtained for a given magnetic core reference. Column D describes the sub-optimal achieved by the algorithm regarding E58 core reference. Obviously, one DAB sizing stands out from the others by achieving a very attractive power to weight ratio. Indeed 4.5 kW/kg is a very high level of performance twice higher than standard DAB implementation, the typical classic figure being close to 2.0 kW/kg. Besides this key piece of information, a number of further lessons can be drawn from the results analysis that bear mention.

- The best parameters set is in the middle of the search space and not at its borders, which clearly suggests that the addressed problem has a real optimal solution rather than a constrained solution.
- The best power-to-weight ratio far exceeds state-of-the-art. The optimal option (column B) achieves much higher level of performance than previous implementations do. It implies that GaN transistors are real game changers for future developments.
- The various switching frequencies are set high to limit the inductance and transformer masses. Using E64 core however induces such high LV currents as well as significant parasitic windings capacitor increase that the algorithm tends to significantly limit the switching frequency. This limitation hence negatively impacts the power-to-mass ratio. Similarly a smaller core like E43 core has a limited performance index. Indeed, lowering the LV currents mechanically reduces copper losses and enables to increase the switching frequency, which unfortunately boosts side GaN driving energy and core losses. The related global performance (column A) is significantly lower than the best sizing based on E58 core (column B).

- The sub-optimal sizing using an E58 ferrite core (column D) shows the trade-off between power density and efficiency. The increase in the number of paralleled transistors in the bridges enables to reduce the conduction losses at the cost of a higher mass. This sizing has a lower power density, but enables to gain 0.5 points of efficiency in comparison with the optimal design (column B).
- Two winding configurations stand out. The partial interleaving configurations (S-P-P-S-S-P-P-S-S-P[1] (c1) and P-S-S-P-P-P-S-S-P (c2)) are the most suitable because they perform well regarding AC resistance while limiting the value of the transformer parasitic capacitance C_p. This low value permits to achieve high resonant frequency and hence high switching frequency.
- Although very appropriate for high frequency operation, the planar transformer remains a key component. The optimization algorithm chooses a set of parameters maximizing the transformer RMS currents while the thermal constraint. This latter is achieved based on a global minimization of core and copper losses.
- Core and copper transformer losses are generally not balanced. Indeed, to reduce the transformer and inductor sizes, the switching frequency should be increased. In a specific frequency bandwidth, core losses may be reduced. For instance core losses of 3C95 Ferroxcube ferrite are reduced in the [100 - 500]kHz bandwidth. Conversely increasing the switching frequency may significantly boost copper losses. Skin and proximity effects indeed impact substantially these losses. However, current magnitude should be high to reach a high converter power rating. So this is why the overall optimization process favors higher copper losses than core ones.
- These very encouraging results should now be refined to consider EMC filters.

Table 3: Parameter sets maximizing the power mass density of the elementary conversion brick.

Parameters	**Optimal Solutions**			**Sub-optimal solution**
P_m (kW/kg)	3.78	4.47	4.1	4.08
P (kW)	1.01	1.92	2.4	1.99
η (%)	97.46	97.7	97.9	98.2
f (kHz)	410	304	176	272
L (μH)	22.8	16.2	22.4	17.5
core reference	E43/10/28-3C95	E58/11/38-3C95	E64/10/50-3C95	E58/11/38-3C95
Winding configuration	(c2)	(c1)	(c1)	(c1)
Resonant frequency (kHz)	1448	1090	632	1020
$P_{tr,core}$ (W)	4.4	3.64	2.2	3.9
$P_{tr,copper}$ (W)	3	8.0	11.3	7.8
e (μm)	140	175	210	210
d_{ps} (μm)	470	535	275	470
$d_{pp} = d_{ss}$ (μm)	325	230	200	250
e_0 (μm)	125	210	270	190
HEMT HV reference	GS66516T	GS66516T	GS66516T	GS66516T
HEMT LV reference	EPC2020	EPC2020	EPC2020	EPC2020
N_1	1	2	2	3
N_2	2	4	6	6

[1]This notation means that the winding (c1) is composed of 10 layers of conductor. Layers 1, 4, 5, 8 and 9 are for the secondary winding, and layers 2, 3, 6, 7 and 10 are for the primary winding. The numbers correspond to those defined in Figure 5.

5.4. Prototype and first experimental results

The DAB candidate sizing comprehensive study offers promising prospects to achieve compact insulated DC-DC power converters. Before moving to the industrial development stage, electronic designers have to validate implementation hypotheses. In particular, dedicated research teams have to check that at least four GaN transistors may be driven using the same gate driver and routed with insignificant parasitic inductances and low resistive connections. Additionally, the carrying out should also validate the thermal management based on a single heat-sink per bridge. Regarding the planar transformer, experimental trials have to assess parasitic capacitor value and global losses at various powers.

For these specific purposes, the HV (i.e. 270V) and LV (i.e. 28V) bridges have been implemented based on GaN Systems and EPC components, respectively (Fig. 8). Planar transformers have also been developed, manufactured and tested. These elements are meant to be assembled to constitute a DAB, with a rated power of 1.9 kW and operating at a frequency of 304 kHz. Experimental basic tests have demonstrated the feasibility of i) parallelization of GaN components (4 on the LV bridge and 2 on the HV bridge), ii) bridges thermal management using a single heatsink and iii) the planar HF transformer high-quality performance, even with large current ratings.

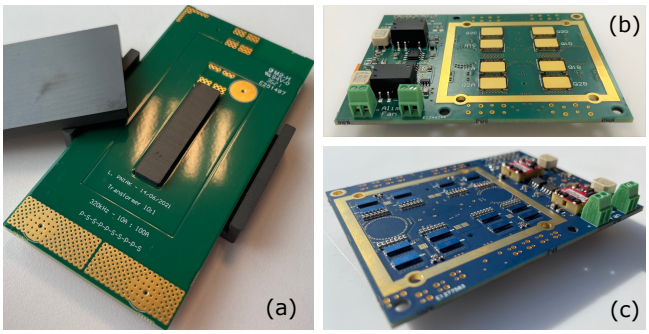

Figure 8: (a) Transformer, (b) HV bridge, (c) LV Bridge.

Thanks to the planar transformer prototype, we were able to validate the original model for estimating the AC resistance of the windings, presented in section 3 of this paper. Figure 9a shows the winding resistance as a function of frequency. We observe a difference of about 15% between the measurement and the model estimate at the frequency of 300kHz. This discrepancy is probably due to the 3D effects of the transformer which are not taken into account in our 2D analytical model. This is supported by Figure 9b, which shows the estimation of the winding resistance as a function of frequency by the analytical model and by 2D finite element simulation for different winding interleaving. The deviations here are very small and show that the analytical model is accurate and quick, which makes it perfectly suited for optimization.

Finally, it can be noted that the overall mass objective was successfully achieved. Table 5 compares the masses estimated by the algorithm for the optimal DAB (Table 4, column B) and the actual measured masses of the different components shown in Figure 6.

Table 4: Mass estimation and comparison.

Component	Estimated	Measured
LV Bridge	115 g	130 g
HV Bridge	96 g	100 g
Transformer	185 g	180 g
Inductance	37 g	50 g
TOTAL	433 g	460 g

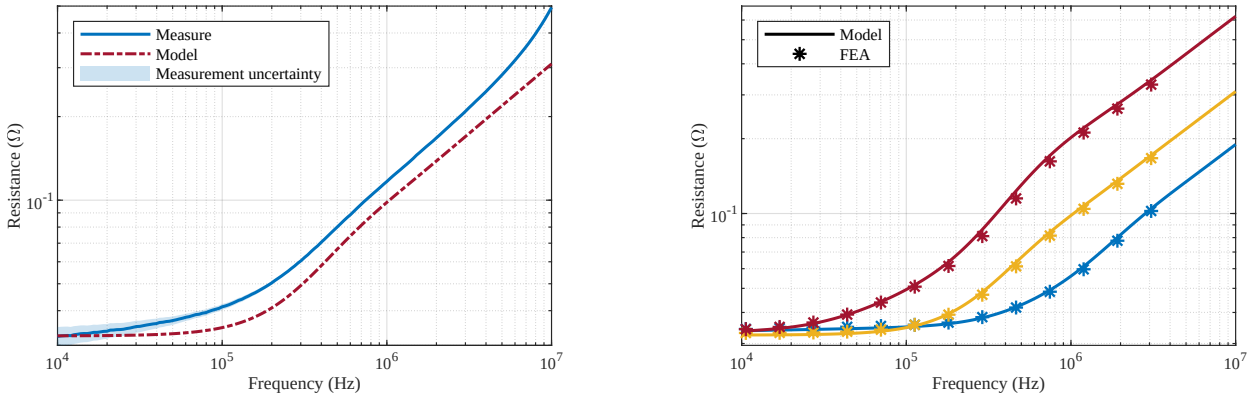

Figure 9: Winding resistance of the transformer as a function of frequency. (a) Comparison of the estimation of the proposed analytical model used for the DAB optimization with measurements conducted with the actual transformer presented on Figure 8. (b) Comparison between 2-D FEA simulations (asterisk markers) and the analytical model (solid lines) for the configurations P-S-P-S-P-S-P-S-P-S (fully interleaved in blue), P-S-S-P-P-S-S-P-P-S (partially interleaved 1 in yellow), and P-P-S-S-S-P-P-P-S-S (partially interleaved 2 in red).

6. Conclusion and perspectives

The MEA development still faces challenges to achieve aircraft auxiliary power fully based on electrical energy. Among identified issues stands the proof that switching to this form of energy is attractive in terms of reducing the mass and volume of the complete system. The present work was carried out with a view to providing an electronic power converter sizing tool enabling to accurately assess mass and losses. It is intended to be precise, rapid and generic at the same time. These specifications therefore make it possible to explore a large research domain, and therefore to carry out an exhaustive search for the best converter, i.e. the one maximizing the chosen objective function. It also makes it possible to regularly examine the optimum defined regarding the evolution of the technological characteristics of the various components used in the power converter.

For this purpose, the current study has developed analytical models of all the components implemented in the power converter, including, in particular, the HF transformer ensuring the crucial galvanic isolation function. The models could be validated during the realization of the converter obtained as an optimization process output. The case study chosen is deliberately difficult to implement and model while being particularly vital in the distribution of electrical energy within the aircraft. Based on a mono-objective optimization process (the power-to-weight ratio), the converter obtained has an attractive performance index (4.5 kW/kg, without considering EMI filters) compared to standard converters ($\sim$ 2 kW/kg). This disruptive result is essentially due to the integral use of novel GaN components. These are connected in parallel both in the low and high voltage sides. The capability to integrate this parallelization without any extra parasitic inductance while using the same driver for each parallel switches has been fully tested on a full scale implemented prototype.

Based on these main achievements, the prospects of this work are to combine the elementary bricks so as to obtain and test the main function, i.e. LV and HV buses connection. From a methodological point of view, it seems valuable to extend the current modeling to take into account aging phenomena, making it possible to assess the function reliability as well as the required level of maintenance.

References

[1] M. Tahir, S. Ahmed Khan, T. Khan, M. Waseem, D. Khan, A. Annuk, More electric aircraft challenges: A study on 270 V/90 V interleaved bidirectional DC–DC converter, Energy Reports 8 (2022) 1133–1140. doi:10.1016/j.egyr.2022.06.084.

[2] J.-C. Maré, J. Fu, Review on signal-by-wire and power-by-wire actuation for more electric aircraft, Chinese Journal of Aeronautics 30 (2017) 857–870. doi:10.1016/j.cja.2017.03.013.

[3] A. Wileman, S. Aslam, S. Perinpanayagam, A road map for reliable power electronics for more electric aircraft, Progress in Aerospace Sciences 127 (2021) 100739. doi:10.1016/j.paerosci.2021.100739.

[4] G. Buticchi, S. Bozhko, M. Liserre, P. Wheeler, K. Al-Haddad, On-Board Microgrids for the More Electric Aircraft—Technology Review, IEEE Transactions on Industrial Electronics 66 (2019) 5588–5599. doi:10.1109/TIE.2018.2881951.
[5] G. Buticchi, L. F. Costa, M. Liserre, Multi-port DC/DC converter for the electrical power distribution system of the more electric aircraft, Mathematics and Computers in Simulation 158 (2019) 387–402. doi:10.1016/j.matcom.2018.09.019.
[6] H. Ounis, B. Sareni, X. Roboam, A. De Andrade, Multi-level integrated optimal design for power systems of more electric aircraft, Mathematics and Computers in Simulation 130 (2016) 223–235. doi:10.1016/j.matcom.2015.08.016.
[7] S. S. Trivedi, A. V. Sant, Comparative analysis of dual active bridge dc–dc converter employing Si, SiC and GaN MOSFETs for G2V and V2G operation, Energy Reports 8 (2022) 1011–1019. doi:10.1016/j.egyr.2022.08.100.
[8] F. Boige, F. Richardeau, S. Lefebvre, M. Cousineau, SiC power MOSFET in short-circuit operation: Electro-thermal macro-modelling combining physical and numerical approaches with circuit-type implementation, Mathematics and Computers in Simulation 158 (2019) 375–386. doi:10.1016/j.matcom.2018.09.020.
[9] A. M. Naradhipa, S. Kim, D. Yang, S. Choi, I. Yeo, Y. Lee, Power Density Optimization of 700 kHz GaN-Based Auxiliary Power Module for Electric Vehicles, IEEE Transactions on Power Electronics 36 (2021) 5610–5621. doi:10.1109/TPEL.2020.3026328.
[10] J. Lu, K. Bai, A. R. Taylor, G. Liu, A. Brown, P. M. Johnson, M. McAmmond, A Modular-Designed Three-Phase High-Efficiency High-Power-Density EV Battery Charger Using Dual/Triple-Phase-Shift Control, IEEE Transactions on Power Electronics 33 (2018) 8091–8100. doi:10.1109/TPEL.2017.2769661.
[11] S. Kenzelmann, A. Rufer, D. Dujic, F. Canales, Y. R. de Novaes, Isolated DC/DC Structure Based on Modular Multilevel Converter, IEEE Transactions on Power Electronics 30 (2015) 89–98. doi:10.1109/TPEL.2014.2305976.
[12] M. González, V. Cárdenas, H. Miranda, R. Álvarez Salas, Modular multilevel converter for large-scale photovoltaic generation with reactive power flow and unbalanced active power extraction capabilities, Mathematics and Computers in Simulation 162 (2019) 135–154. doi:10.1016/j.matcom.2019.01.007.
[13] R. Vidal, D. Soto, I. Andrade, J. Riedemann, C. Pesce, E. Belenguer, R. Pena, R. Blasco-Gimenez, A multilevel modular DC–DC converter topology, Mathematics and Computers in Simulation 131 (2017) 128–141. doi:10.1016/j.matcom.2015.12.004.
[14] M. Blanc, Y. Lembeye, J.-P. Ferrieux, C. Rizet, A. Mahe, T. Bensalah, Optimization of a DC/DC dual active bridge converter for aircraft application, EPE Journal 28 (2018) 182–199. doi:10.1080/09398368.2018.1489482.
[15] J. C. Brandelero, Conception et réalisation d'un convertisseur multicellulaire DC/DC isolé pour application aéronautique, Phd Thesis, INP de Toulouse, 2015.
[16] M. Forouzesh, Y. P. Siwakoti, S. A. Gorji, F. Blaabjerg, B. Lehman, Step-Up DC–DC Converters: A Comprehensive Review of Voltage-Boosting Techniques, Topologies, and Applications, IEEE Transactions on Power Electronics 32 (2017) 9143–9178. URL: http://ieeexplore.ieee.org/document/7872494/. doi:10.1109/TPEL.2017.2652318.
[17] F. Krismer, Modeling and optimization of bidirectional dual active bridge DC-DC converter topologies, Ph.D. thesis, ETH Zurich, 2010. doi:10.3929/ETHZ-A-006395373.
[18] F. Teng, D. Kong, Z. Cui, Y. Qin, Z. Hao, N. Rong, Z. Chen, DCSST Multi-Modular Equalization Scheme Based on Distributed Control, Sensors 21 (2021) 8125. URL: https://www.mdpi.com/1424-8220/21/23/8125. doi:10.3390/s21238125.
[19] M. Rolak, C. Sobol, M. Malinowski, S. Stynski, Efficiency Optimization of Two Dual Active Bridge Converters Operating in Parallel, IEEE Transactions on Power Electronics 35 (2020) 6523–6532. URL: https://ieeexplore.ieee.org/document/8892643/. doi:10.1109/TPEL.2019.2951833.
[20] J. Aubry, Optimisation du dimensionnement d'une chaîne de conversion électrique directe incluant un système de lissage de production par supercondensateurs : application au houlogénérateur SEAREV, Phd Thesis, École normale supérieure de Cachan, Cachan, 2011.
[21] J. Aubry, H. Ben Ahmed, B. Multon, Bi-objective sizing optimization of a PM machine drive on an operating profile, in: The XIX International Conference on Electrical Machines - ICEM 2010, IEEE, Rome, Italy, 2010, pp. 1–7. doi:10.1109/ICELMACH.2010.5608308.
[22] C. A. Coello Coello, M. Reyes-Sierra, Multi-Objective Particle Swarm Optimizers: A Survey of the State-of-the-Art, International Journal of Computational Intelligence Research 2 (2006). doi:10.5019/j.ijcir.2006.68.
[23] R. De Doncker, D. Divan, M. Kheraluwala, A three-phase soft-switched high-power-density DC/DC converter for high-power applications, IEEE Transactions on Industry Applications 27 (1991) 63–73. doi:10.1109/28.67533.
[24] M. Turzyński, S. Bachman, M. Jasiński, S. Piasecki, M. Ryłko, H.-J. Chiu, S.-H. Kuo, Y.-C. Chang, Analytical Estimation of Power Losses in a Dual Active Bridge Converter Controlled with a Single-Phase Shift Switching Scheme, Energies 15 (2022) 8262. URL: https://www.mdpi.com/1996-1073/15/21/8262. doi:10.3390/en15218262.
[25] G. G. Oggier, G. O. Garcia, A. R. Oliva, Modulation strategy to operate the dual active bridge DC-DC converter under soft switching in the whole operating range, IEEE Transactions on Power Electronics 26 (2011) 1228–1236. doi:10.1109/TPEL.2010.2072966.
[26] G. Lakkas, MOSFET power losses and how they affect power-supply efficiency, Analog Applications Journal (2016) 22–26.
[27] Z. Ouyang, M. A. E. Andersen, Overview of Planar Magnetic Technology—Fundamental Properties, IEEE Transactions on Power Electronics 29 (2014) 4888–4900. doi:10.1109/TPEL.2013.2283263.
[28] J. S. Ngoua Teu Magambo, R. Bakri, X. Margueron, P. Le Moigne, A. Mahe, S. Guguen, T. Bensalah, Planar Magnetic Components in More Electric Aircraft: Review of Technology and Key Parameters for DC–DC Power Electronic Converter, IEEE Transactions on Transportation Electrification 3 (2017) 831–842. doi:10.1109/TTE.2017.2686327.
[29] Z. Ouyang, O. C. Thomsen, M. A. E. Andersen, Optimal Design and Tradeoff Analysis of Planar Transformer in High-Power DC–DC Converters, IEEE Transactions on Industrial Electronics 59 (2012) 2800–2810. doi:10.1109/TIE.2010.2046005.
[30] C. W. T. McLyman, Transformer and inductor design handbook, 4th ed ed., CRC Press, Boca Raton, FL, 2011. OCLC: ocn663445232.
[31] C. P. Steinmetz, On the Law of Hysteresis, Transactions of the American Institute of Electrical Engineers IX (1892) 1–64. doi:10.1109/T-AIEE.1892.5570437.
[32] D. Rodriguez-Sotelo, M. A. Rodriguez-Licea, I. Araujo-Vargas, J. Prado-Olivarez, A.-I. Barranco-Gutiérrez, F. J. Perez-Pinal, Power Losses Models for Magnetic Cores: A Review, Micromachines 13 (2022) 418. doi:10.3390/mi13030418.
[33] P. Dowell, Effects of eddy currents in transformer windings, Proceedings of the Institution of Electrical Engineers 113 (1966) 1387. doi:10.1049/piee.1966.0236.

[34] J. Ferreira, Improved analytical modeling of conductive losses in magnetic components, IEEE Transactions on Power Electronics 9 (1994) 127–131. doi:10.1109/63.285503.
[35] L. Pniak, L. Queval, B. Revol, J.-S. N. Teu, C. Gautier, O. Bethoux, AC Resistance and Leakage Inductance Estimation for Planar Transformers With Parallel-Connected Windings, IEEE Transactions on Power Electronics 38 (2023) 728–738. doi:10.1109/TPEL.2022.3203515.
[36] Wei Chen, Yipeng Yan, Yuequan Hu, Qing Lu, Model and design of PCB parallel winding for planar transformer, IEEE Transactions on Magnetics 39 (2003) 3202–3204. doi:10.1109/TMAG.2003.816147.
[37] R. P. Feynman, The Feynman lectures on physics. Volume II : Mainly electromagnetism and matter, the new millennium edition ed., Basic Books, New York, 2011.
[38] F. P. Incropera, D. P. DeWitt, T. L. Bergman, A. S. Lavine (Eds.), Fundamentals of heat and mass transfer, 6th ed ed., John Wiley, Hoboken, NJ, 2007. OCLC: ocm62532755.